XRM-II nanoCT – SEM based computed tomography

Fabian LUTTER [1], Kilian DREMEL [2], Jens ENGEL [2], Daniel ALTHOFF [2],
Simon ZABLER [2], Nikolas WESTPHAL [3], Randolf HANKE [2]
[1] Chair of X-ray Microscopy LRM, Julius-Maximilians-Universität, Würzburg, Germany
[2] Fraunhofer Development Center X-ray Technology EZRT, Fürth, Germany
[3] ProCon X-Ray GmbH, Sarstedt, Germany

Contact e-mail: fabian.lutter@physik.uni-wuerzburg.de, kilian.dremel@iis.fraunhofer.de,
nikolas.westphal@procon-x-ray.de

Abstract. We present the XRM-II nanoCT, a laboratory nano-CT system based on geometric magnification, which is used for material characterization. The prior system, XRM-II, was presented in 2016 and was the starting point for our development. The new system is composed of a scanning electron microscope JEOL-JSM7900, which is used for focusing electrons on a needle shaped tungsten or molybdenum target with a tip diameter of about 80 nm. In this way we generate a X-ray source spot of the same size to accomplish a spatial resolution below 100 nm. In comparison to the prior system the target can be handled independently from the object stage, while maintaining the full functionality of the SEM. Furthermore, we use a photon counting detector with a 1 mm thick CdTe sensorlayer and a resolution of 1290x512 pixels. The XRM-II nanoCT is also capable of element mapping by using a built-in EDS system. Therefore, the system provides multi-modal imaging using three different image-contrasts (SEM, EDS, nano-CT) on the same sample.

The acquisition time for a CT, consisting of 1200 projections, is about 34 hours. By using image correlation to compensate the problem of electron beam drift, the data acquisition is fully automated. Due to the high spatial resolution, sample-drift and positioning inaccuracies need to be compensated during the CT reconstruction. A customized algebraic reconstruction method allows to improve the low signal-to-noise ratio of the CT projections by regularization and to get rid of geometric deviations.

We present details about the experimental setup, high resolution radiographies and reconstruction results of a 3D nano-CT of a metallic alloy.

1. Introduction

Nano-CT resolves structures in the range of a few hundred nanometers to some micrometers. This volumetric imaging technique is important for material scientists, because the characteristics and behaviour of materials is often defined by their microstructure [1]. By the means of electron microscopy, it is possible to examine the surface of a sample with a resolution of a few nanometers, but information from more than few hundreds of nanometers beneath the surface is not accessible. To gain volumetric information of the sample FIB tomography or nano-CT can be used. We presented a laboratory based nano-CT system (XRM-II) in 2016, based on geometric magnification [2]. A spatial resolution in 2D of 3000lp/mm could be achieved with this system, while there was less resolving power in volumetric imaging due to limitations in the signal-to-noise-ratio (SNR). The previous

acquisition time of 10-14 days for the computed tomography was quite long and the functional range of the SEM was limited due to the nano-CT setup. In this work we show the improvements made compared to the prior system and give an impression on its functional capabilities by recording an AlCu29 alloy.

2. Materials and Methods

2.1 Principle of geometric magnification

The XRM-II nanoCT system is based on the principle of geometric magnification. The magnification M is given by the source-detector distance z_1 and the source-object distance z_2:

$$M = \frac{z_1}{z_2}$$

The size of the X-ray source is an important point to achieve high resolution [2]. To keep the source spot as small as possible, the electron interaction volume of the reflection target must be reduced to a minimum. A larger spot size will cause a blurring of the image at the same magnification [2].

2.2 X-ray targets

Our approach to reduce the electron interaction volume results in the use of needle shaped reflection targets, which are made of tungsten or molybdenum. We use an electrochemical etching process to create these targets with a tip diameter of less than 100nm [3], [4]. This process is tuned to fulfill the important attributes like shape, stiffness, conductivity and thermal resistance.
A SEM image of a tungsten target is shown in Fig. 1. The electron beam is focused on the very end of the tip, where the diameter is about 80nm. Multiple nano-CTs were performed with this target and it shows no damage caused by the high electron current (~400nA).

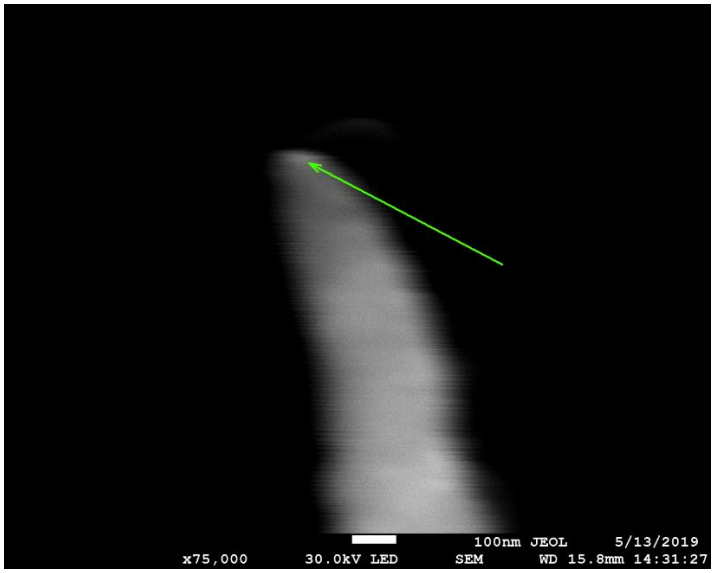

Fig. 1. SEM image of the needle-shaped tungsten target; The green arrow marks the point where the electron beam is focused on to create the X-ray source.

2.3 Experimental setup

The XRM-II nanoCT is based on a field emission scanning electron microscope JEOL JSM-7900. It is capable of high resolution in electron imaging (~0,8nm) and is powerful enough to provide high and stable electron flux (~400nA) to generate X-rays. The most significant difference compared to the prior system is the use of two independent manipulators for target and object. Thus, it is possible to use the stage of the SEM to manipulate the object while maintaining the full functional range of the SEM including the use of the specimen exchange mechanism. For the target manipulator we use a stack of three linear axes, which is attached on the inside of the specimen chamber. As shown in Fig. 2, object and target are inside the vacuum chamber of the SEM, while the X-ray detector is placed outside the microscope behind a 250µm thick Beryllium window. The detector is a photon counting ADVACAM WidePIX with a 1mm thick CdTe sensor layer and a 1290x512 pixel matrix with a pixel size of 55µm. This offers a field of view of 100µm with 80nm sampling. Furthermore, an EDS detector is attached to get information of the sample's elemental composition.

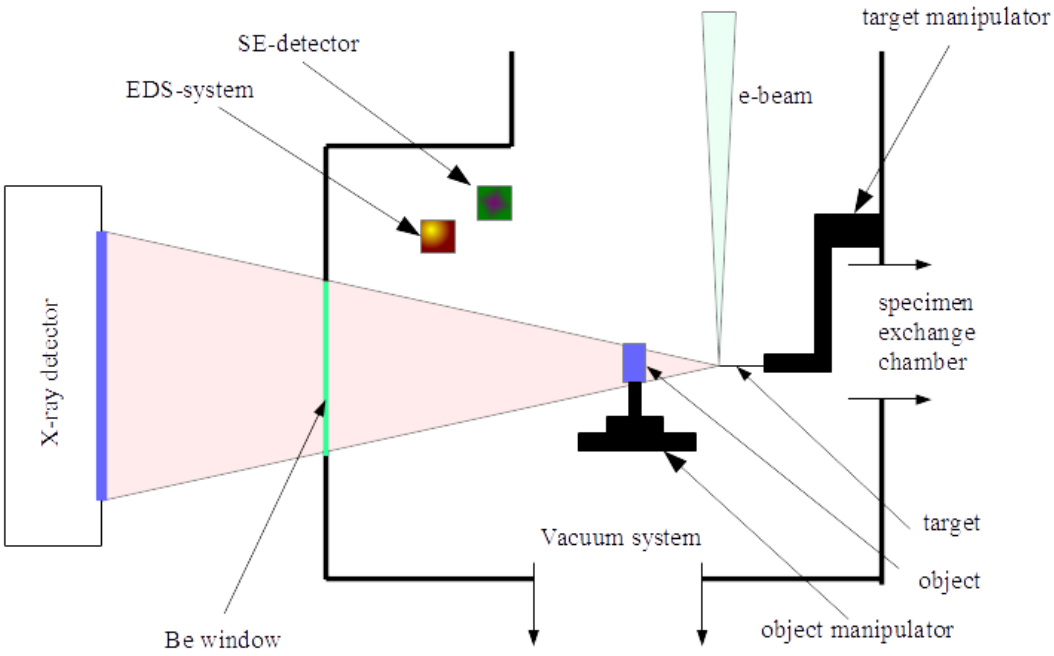

Fig 2. Schematic representation of the specimen chamber; Compared to the prior system, object and target manipulator are now separated, which makes the system easier to use and keeps the complete functional range of the SEM available.

The 30kV electron beam is focused on a needle-shaped tungsten tip with tip diameters less than 100nm (see Fig. 1). This creates an X-ray spot of the same size**.** The resulting X-ray spectrum, collected with the EDS-system, is shown in Fig. 3. The main peaks are the fluorescence lines of tungsten at $W_{L\alpha}$=8,40keV, $W_{L\beta}$=9,67keV, $W_{L\gamma}$=11,29 keV [5].

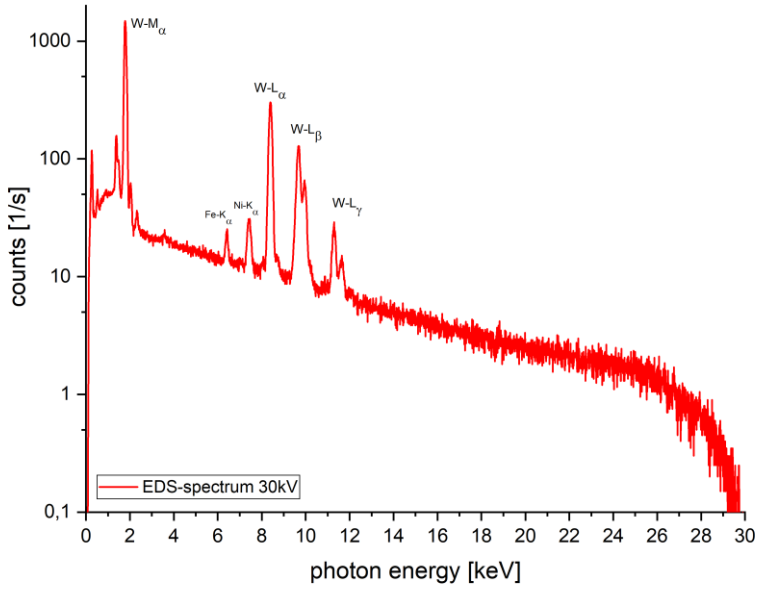

Fig. 3. X-ray Bremsspektrum of the tungsten tip; The peaks originate from the Wolfram fluorescence lines. Photons lower than 5keV don't reach the detector due to the Beryllium window.

The remaining lines of iron and nickel originate from a secondary X-ray spot on the sample stage caused by the transmitted electrons, which were not absorbed by the target. The intensity below 5keV is almost completely cut off by the Be-window, which is why the lower energy threshold of the detector is set to the this energy.

Charging effects of the sample and changing electrical fields during stage movements, especially rotations, cause a misalignment of target and electron beam, which leads to a breakdown of the X-ray intensity. To prevent this, the electron beam is realigned by using image correlation of SEM images during the CT process [6]. Hereby, the CT procedure was fully automated and requires no user interaction.

2.4 Volume data reconstruction

The 3D volume of XRM-II nanoCT data is computed by a custom designed software (see also [2]), which includes a consideration of the typical measurement setup, a compensation for mechanical instabilities and a 3D phase-contrast filter. Since the photon flux is low due to the small focal spot size and the signal-to-noise ratio (SNR) is critical, a regularized reconstruction method is needed to achieve good results. Iterative volume reconstruction gives the possibility to not only include regularization but also deal with the non-equidistant angular setup of the XRM-II nanoCT. We use a total-variation (TV) [10] regularized Simultaneous Algebraic Reconstruction Technique (SART) [7] reconstruction algorithm. Moreover, geometric deviations occur due to the high magnification of the system. Since smallest mechanical instabilities and thermal drift of a few nanometers lead to non-negligible errors in the geometry, an image-correlation based correction compares the forward-projected volume image to the measured data in order to detect sample shifts in the detector plane (see also [11], [8]).

After the reconstruction a Paganin based phase contrast filter [9] is applied in the volume space to get images with better contrast. To deal with the intrinsic blurring by the Paganin Filter, a second deconvolution filter is used.

3. Results

In order to demonstrate the achievable resolution in 2D, we used a Siemens star as a test pattern. The magnification for this measurement was set to 5500x corresponding to a sampling of 10nm per pixel (see Fig.4). The lines of the ring numbered as 3 have a feature width between 176nm and 80nm. These features are clearly resolved, while smaller lines in the following inner ring are also visible.

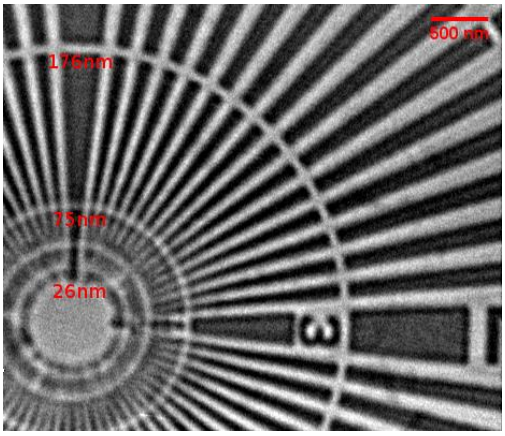

Fig. 4. Radiography of Siemens star recorded with a Magnification of 5500x or 10 nm pixel sampling and an integration time of 30 minutes. Details down to 80nm are clearly distinguishable, while smaller features are also visible.

We chose an AlCu29 alloy as our sample to analyse with the system and compare the results to our previous measurement of this alloy. Furthermore, its internal structures are in the range of the system's achievable resolution and provide a good contrast for X-ray imaging. First, we recorded a SEM image of the sample (Fig. 5). The grooves on the surface of the sample originate from the preparation with fine sandpaper as well as the light particles on the top.

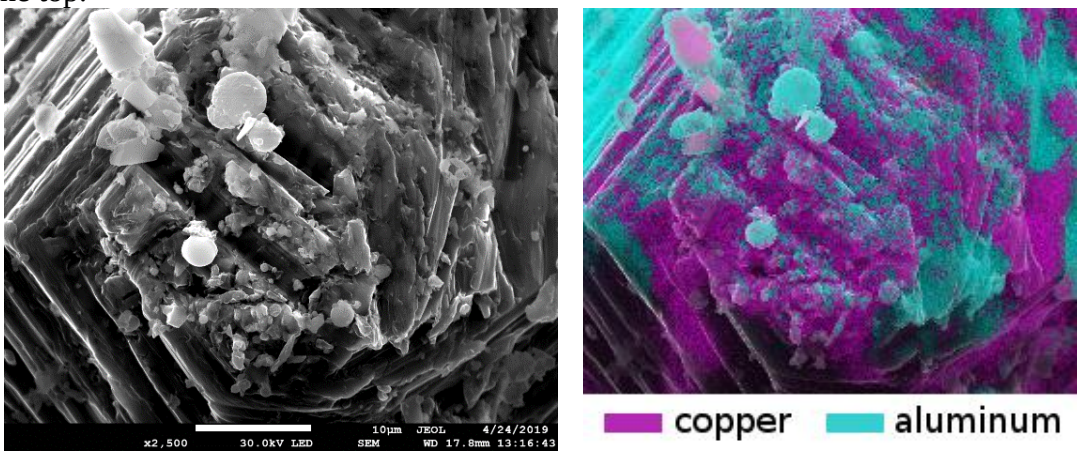

Fig. 5. SEM and EDS image of the sample: (left image) The bright particles are remnants of sandpaper used during the preparation. The light and dark areas on the upper right of the sample are two different metallic phases of the alloy. (right image) In the map, coloured by the EDS-system, aluminum is represented in turquoise, while copper is purple. Both phases are visible on the sample surface. The spheres on top were identified as silicon but excluded from the mapping. The dark areas in the lower left part are caused by the conical shape of the sample shielding the EDS-detector.

We performed an EDS mapping to determine the elemental distribution of the sample. Fig. 5 shows the expected metals (aluminum and copper) and the remnants of sandpaper (silicon dioxide).

The subsequent nanoCT-scan was performed with 1000 projections 100s exposure time each and a magnification of M=585. In total, the acquisition time was about 34 hours.

Slices of the reconstructed and the Paganin-filtered volume (94nm voxel size) as well as line plots of the eutectic structure are shown in Fig. 6.

The Al-Al2Cu eutectic phase with a periodicity of about 1µm is clearly visible. Furthermore, aluminium particles with a size of 20-30µm are present. The finest lamination of the intermetallic phase is about 350nm large. The small sphere on top of the sample, which was identified as Silicon dioxide by the EDS, is also visible in the reconstructed volume as well as the grooves on the surface caused by sample-preparation with sandpaper.

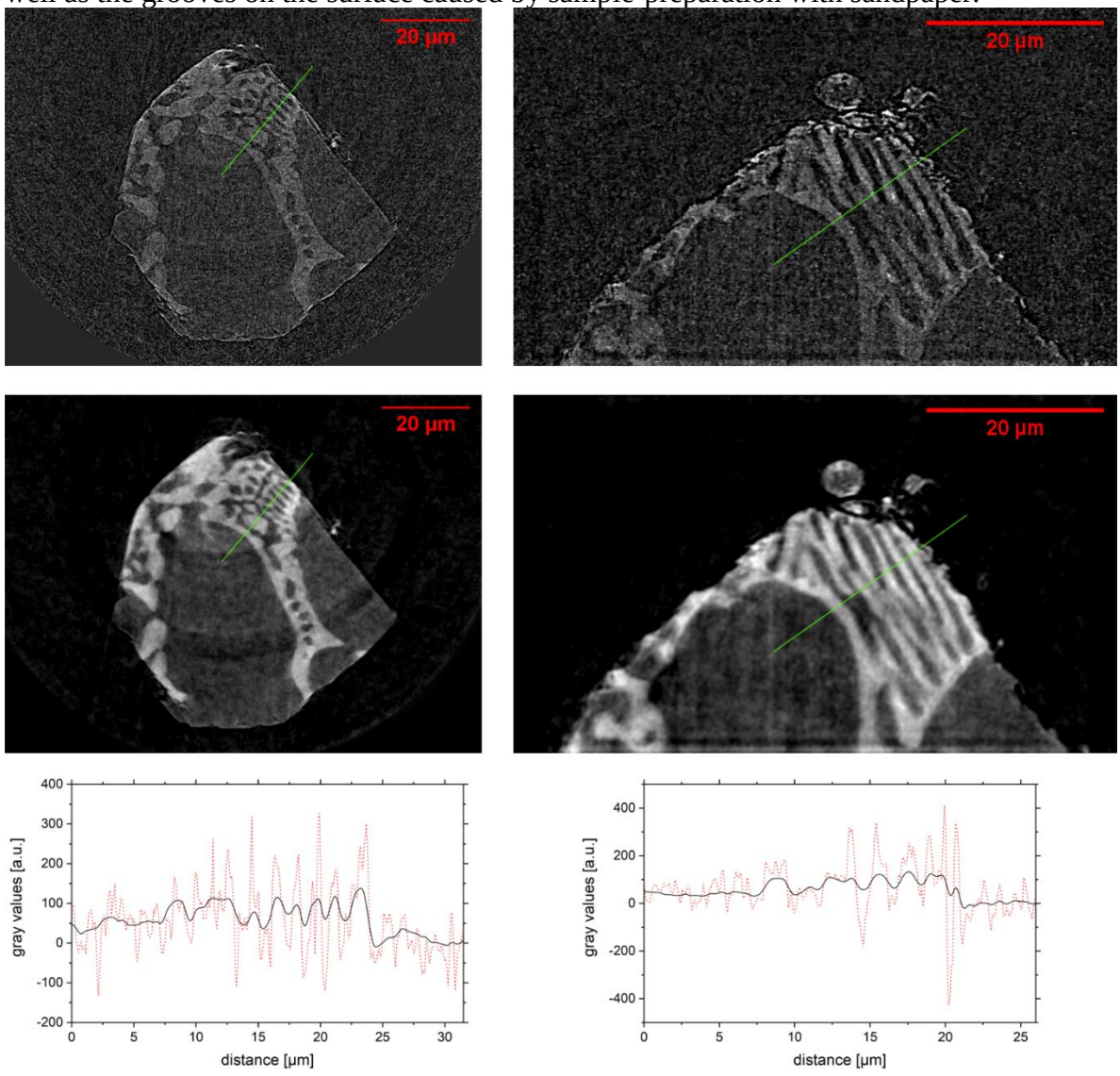

Fig. 6. Reconstruction results of the AlCu29 alloy; Slices of the unfiltered results are shown in the first line, while the Paganing-filtered ones are in the second line. In the line plots along the green lines, phase overshoots can be seen in the unfiltered image (red dashed line), while the filtering smooths the results (black solid line).

We used the FWHM of the derivative of the line profile at the eutectic microstructure to estimate the line spread and the corresponding resolution. For the unfiltered volume, we find a line spread between 1,5 and 2,7 pixels corresponding to a resolution of 135nm – 255nm. In the phase retrieved volume the line spread is between 3 and 4 pixels, which equals to a resolution of 270nm – 360nm. The unfiltered volume offers the better resolution, while the Paganin-filtered one has an improved image contrast.

4. Conclusions and Outlook

The XRM-II nanoCT system provides three different image contrast mechanisms of the same sample. The SEM- and EDS-image can be used for high resolution surface analysis and determination of the constituting elements, while the nano-CT provides additional volume information of the sample.

Due to our improvements in comparison to the prior XRM-II system, it became much faster and easier to use. The total acquisition time for a nano-CT was shortened from 10-14 days to 1,5 days by using a significant higher electron beam current due to optimized parameters of the SEM. By using the alignment between electron beam and target, the acquisition for the computed tomography is now fully automated. The use of two independent motor stages for object and target made the system more user-friendly and maintained the full functionality of the SEM, especially the built-in exchange mechanism. The usable magnification range in X-ray-mode varies from 100x to 1000x (550nm – 55nm voxel size) for computed tomography and up to 5500x (10nm pixel size) for radiographic imaging.

The XRM-II nanoCT system can be used to characterize metallic alloys, but is also capable of examining organic samples or micro electronic devices. Organic samples must be coated with a few nanometer thick layer of gold or carbon to minimize charging effects and electron beam drift.

There are already two systems running and in use in Saarbruecken at the ZRM and in Fuerth at the Fraunhofer EZRT. Both are distributed by ProCon X-Ray GmbH, while a third one is located at the chair of X-ray microscopy in Würzburg using the SEM of the prior system with the new manipulator setup.

In the future it will be possible to further shorten the acquisition time for the CT by increasing the beam current. The currently used JSM-7900 supports currents up to 1µA, which would increase the X-ray intensity by a factor of 2. Furthermore, the design of the target manipulator allows the mounting of up to 4 different targets. In this way, it will possible to switch the target material without venting the specimen chamber of the SEM.

References

[1] C.H.McMurtry, W.D.G.Boecher, S.G.Seshadri, J.S.Zanghi, J.E.Garnier “Microstructure and material properties of SiC-TiB_2 particulate composites. United States: N. p., 1987. Web.

[2] P.Stahlhut, K.Dremel, J.Dittmann, J.M.Engel, S.Zabler, A.Hoelzing, R.Hanke “First results on laboratory nano-CT with a needle reflection target and an adapted toolchain”, Proc. SPIE 9967, Developments in X-Ray Tomography X, 99670l (3 October 2016); doi: 10.1117/12.2240561

[3] M.Fotino, “Tip sharpening by normal and reverse electrochemical etching”, Rev. Sci. Instrum 64, 159-167 (1992)

[4] W.-T.Chang, I.-S.Hwang, M.-T.Chang, C.-Y.Lin, W.-H.Hsu, J.-L.Hou “Method of electrochemical etching of tungsten tips with controllable profiles,” ”, Rev. Sci. Instrum 83, 083704 (2012)

[5] A.Thompson, D.Attwood, E.Gullikson, et. Al. “X-ray data booklet”, 2009

[6] F.Lutter “Anwendungen für ein Laborbasiertes Nano-CT System,” Master Thesis Universität Würzburg (2017)

[7] A.H.Andersen and A.C.Kak, "Simultaneous algebraic reconstruction technique (SART): a superiorimplementation of the ART algorithm," Ultrasonic imaging 6.1, 81-94 (1984)

[8] S.Mayo, P.Miller, D.Gao and J.Sheffield-Parker, "Software image alignment for X-ray microtomography with submicrometre resolution using a SEM-based X-ray microscope," Journal of Microscopy 228.3, 257-263(2007)

[9] D.Paganin, S.C.Mayo, T.E. Gureyev, P.R Miller and S.W.Wilkins, "Simultaneous phase and amplitude extraction from a single defocused image of a homogeneous object," Journal of microscopy 206.1, 33-40 (2002)

[10] E.Y.Sidky, C.M.Kao and X.Pan, "Accurate image reconstruction from few-views and limited-angle data in divergent-beam CT," Journal of X-ray Science and Technology 14.2, 119-139 (2006)

[11] K.Dremel, D.Althoff, and S.Zabler, "CT alignment correction in iterative reconstruction methods," Proc. 4thIntl. Mtg. on image formation in X-ray CT 40, 137 (2016)